DOI: https://doi.org/10.15407/pmach2026.01.016

UDC 539.3

EFFECT OF CARBON NANOTUBE EMBEDDING ON THE MECHANICAL PROPERTIES OF DELAMINATED CARBON FIBER REINFORCED POLYMER COMPOSITE PLATES

Muhammad Imran
muhammad.imran@iiu.edu.pk,
ORCID: 0000-0002-2704-6813

International Islamic University,
Islamabad 44000, Pakistan

Carbon fiber reinforced polymer (CFRP) composites are widely employed in aerospace, automotive, and civil infrastructure applications owing to their exceptional specific stiffness and strength. Delamination is one of the critical parameter in composite materials. However, interlaminar delamination remains the predominant failure mode critically undermining structural integrity. The present study investigates the influence of multi-walled carbon nanotube (MWCNT) reinforcement, introduced via matrix-level dispersion, on the mechanical response of CFRP laminates with pre-existing circular delaminations of varying diameters (10, 20, and 30 mm) at the mid-plane. Quasi-isotropic $[0/45/-90/-45]_s$ laminates (nominal thickness 4 mm) were fabricated by vacuum-assisted resin infusion. Three MWCNT weight fractions (0, 0.3, and 0.5 wt.%) were examined. Specimens were characterised by tensile, compressive, short-beam shear, mode-I double-cantilever beam fracture, and compression-after-impact tests. Digital image correlation was employed to map full-field strain distributions. Incorporation of 0.3 wt.% MWCNTs increased ILSS by 18.3%, mode-I G^Ic by 34.4%, and compression-after-impact strength by 22.0% relative to neat CFRP with equivalent delamination. At 0.5 wt.%, agglomeration effects partially offset these gains. Fractographic SEM revealed carbon nanotube pull-out, crack bridging, and matrix micro-crack deflection as operative toughening mechanisms. These findings demonstrate that low-concentration MWCNT doping constitutes an effective strategy for mitigating delamination-induced degradation in CFRP structural panels.

Keywords: *carbon nanotube, carbon fiber reinforced polymer, delamination, interlaminar fracture toughness, short-beam shear, compression-after-impact, digital image correlation, toughening mechanism, epoxy nanocomposite.*

1 Introduction

Carbon fiber reinforced polymer (CFRP) composites have become indispensable structural materials across a broad spectrum of engineering sectors, including aeronautical primary structures, wind-turbine blades, high-performance automotive chassis, and pressure vessels for hydrogen storage [1, 2]. The CFRP global market was projected to reach $32 billion by 2025, with production forecast to grow continuously driven by electrification of aviation and expansion of offshore wind capacity [3]. The combination of high specific modulus, fatigue resistance, and corrosion immunity renders CFRP superior to metallic alloys in weight-critical design. Despite these advantages, laminated CFRP exhibits an inherent vulnerability: interlaminar delamination—separation of adjacent plies along the resin-rich interlaminar zone.

Delamination may be initiated by low-velocity impacts, manufacturing defects such as resin-starved regions, edge-stress concentrations, or cyclic fatigue loading [4, 5]. Imran et al. [6] provided a comprehensive review of failure modes in laminated composites and identified interlaminar delamination as the most critical and frequently encountered defect type in service. Once formed, a delamination propagates under compressive or shear loads, causing dramatic knockdown in structural stiffness and load-carrying capacity; sublaminate buckling above the delamination boundary can reduce compressive residual strength by up to 60% for moderate impact energies [7]. Li et al. [8] experimentally confirmed that delamination defects drastically reduce both tensile and compressive properties of CFRP, with the degree of degradation strongly dependent on delamination size and through-thickness location. Calvo et al. [9] further demonstrated using 3D digital image correlation (DIC) that CFRP plates with mid-plane delamination exhibit global and local buckling modes whose relative contribution is governed by delamination extent.

The dynamic consequences of delamination have been systematically characterised by Imran et al. [10–12] in a series of experimental and computational studies. Their work demonstrated that both delamination size and stacking sequence significantly reduce natural frequencies of CFRP plates, with mid-plane de-

lamination producing the greatest frequency reductions. The finite element study of Imran et al. [12] confirmed that the interplay between boundary conditions and delamination geometry controls the magnitude of structural stiffness degradation. More recently, Imran et al. [13] extended this framework to clamped-clamped boundary conditions, demonstrating that this configuration produces larger frequency knockdowns than simply supported plates for equivalent delamination areas. These dynamic characterisation results collectively motivate the development of matrix-level modifications capable of arresting delamination growth and limiting stiffness degradation during service.

The inherently low through-thickness properties of continuous-fiber composites originate from the absence of reinforcement perpendicular to the lamination plane. Conventional toughening strategies include z-pinning, 3D weaving, stitching, and thermoplastic veil interleaving [14, 15]. The advent of carbon nanotubes (CNTs) offered a conceptually elegant alternative: nanoscale reinforcement capable of bridging crack faces, deflecting microcracks, and transferring load across interlaminar interfaces without perturbing the macroscopic fiber architecture. Carbon nanotubes, first described by Iijima in 1991 [16], combine a Young's modulus approaching 1 TPa with tensile strengths exceeding 60 GPa [17]. Multi-walled carbon nanotubes (MWCNTs) are available at industrial scale, making them practically attractive for aerospace-grade CFRP manufacture.

Early studies by Thostenson and Chou [18] demonstrated that CNTs enhanced compressive strength of aligned CFRP. Bekyarova et al. [19] reported 30% ILSS increases using functionalised single-walled carbon nanotubes covalently bonded to carbon fibers. Garcia et al. [20] doubled interlaminar fracture toughness using aligned CNT forests grown directly on woven fabrics. More recent investigations have demonstrated consistent ILSS improvements of 15–25% at 0.1–0.5 wt.% MWCNT loading [21, 22]. Sahu et al. [23] reviewed CNT interface engineering in CFRP and identified crack bridging, pull-out, and matrix micro-crack deflection as the three dominant toughening mechanisms.

Recent high-impact work has further advanced the field. Paiva et al. [24] demonstrated using the J-integral method that aligned CNT interlaminar reinforcement achieves 34% and 62% improvements in mode-I and mode-II initiation fracture toughness, respectively, in thin-ply CFRP, without altering ply thickness or laminate weight. Fulmali et al. [25] achieved enhancements of 73.8% in flexural strength, 58.2% in tensile strength, and 28.5% in ILSS in CFRP through silane-functionalised oxidised MWCNTs. Yin et al. [26] reported that magnetically oriented Z-CNTs at 0.3 wt.% improved mode-I interlaminar fracture toughness by 95.2% in Z-aligned samples, demonstrating the primacy of CNT orientation for maximising toughening efficiency. Sergi et al. [27] showed that MWCNTs significantly toughen quasi-isotropic CFRP laminates under both ambient and sub-zero temperature impact conditions, with residual bending strength improved across all studied temperatures.

On the structural mechanics side, Kolanu et al. [28] characterised full-field deformation and failure of CFRP laminates under compression-after-impact (CAI) using 3D DIC, revealing that delamination-driven local sub-laminate buckling is the critical failure precursor. Xie et al. [29] quantified through uncertainty analysis how micro-defects and delamination compound their effects on CFRP mechanical properties, with delamination area emerging as the dominant variable. Wang et al. [30] demonstrated that hybrid CNT/graphene oxide modifications of CFRP epoxy achieve a synergistic 35% mode-I $G^{I}c$ improvement alongside +12% tensile strength, with molecular dynamics confirming the energy dissipation network formed by the binary nanofiller. Alsheghri and Drakonakis [31] applied machine learning to predict CFRP mechanical properties as a function of CNT volume fraction, establishing a data-driven framework that identified 0.25–0.35 wt.% as the optimal CNT loading window for maximising mode-II energy release rate.

Despite these advances, the combined effect of CNT reinforcement on laminates that already contain delaminations of defined geometry has received scant systematic attention. The present work addresses this gap by systematically characterising the tensile, compressive, interlaminar shear, mode-I fracture, and CAI responses of MWCNT-modified CFRP laminates with mid-plane circular delaminations across three delamination sizes and two MWCNT loadings. DIC strain mapping quantifies delamination-induced strain concentrations and their attenuation by CNT addition. Fractographic analysis identifies operative toughening mechanisms. The study provides quantitative design data relevant to damage-tolerant CFRP structural panels, directly complementing the vibration-based delamination characterisation reported by Imran et al. [10–13].

2 Materials and Methods

2.1 Raw materials and MWCNT dispersion

Plain-weave carbon fiber fabric (Toray T700, 3K tow, areal weight 200 g m^{-2}) was used as reinforcement. The matrix was bisphenol-A epoxy resin (Momentive EPIKOTE 862) cured with cycloaliphatic amine hardener (EPIKURE W) at stoichiometric ratio of 100:26.4 by weight. Pristine MWCNTs (Nanocyl NC7000, outer diameter 9.5 nm, average length 1.5 µm, purity >90%, surface area 250–300 m^2 g^{-1}) were used without chemical functionalisation to reflect industrially relevant practice. Three matrix systems were prepared: neat epoxy (E0), epoxy with 0.3 wt.% MWCNTs (E03), and epoxy with 0.5 wt.% MWCNTs (E05). The MWCNT dispersion and matrix preparation protocol is summarised in Fig. 1.

MWCNTs were first mechanically stirred into the resin at 500 rpm for 30 min at 60 °C, followed by ultrasonication (Hielscher UP400S, 400 W, 24 kHz) for 60 min at 40% amplitude with 2-s intermittent pulse cycles to minimise thermal degradation of the epoxy. The hardener was added under gentle mechanical stirring (100 rpm, 5 min) and the suspension degassed under vacuum (<1 kPa) for 30 min prior to infusion. The zero-shear viscosity at 60 °C was 1.85 Pa·s for E03 (within the vacuum-assisted resin infusion (VARI) processability limit of 2.0 Pa·s) and 2.62 Pa·s for E05, requiring an extended dwell before infusion.

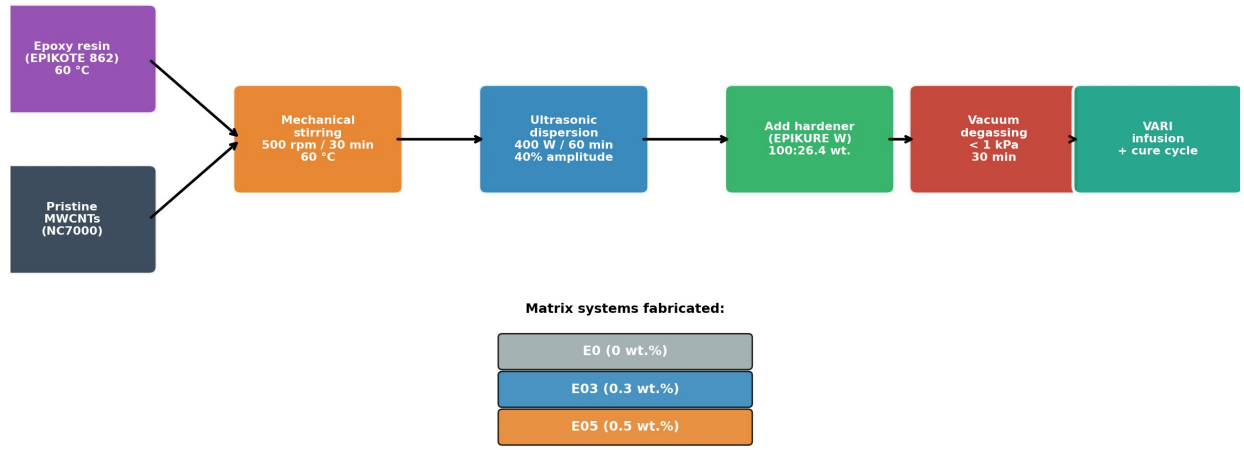

Fig. 1. MWCNT dispersion and matrix preparation protocol for the three matrix systems (E0, E03, E05).
Steps proceed left to right: mechanical stirring → ultrasonication → hardener addition → vacuum degassing → VARI infusion

2.2 Laminate fabrication and delamination introduction

Quasi-isotropic laminates with stacking sequence $[0/45/-90/-45]_s$ (16 plies, nominal thickness 4 mm) were fabricated by VARI on a flat glass tool plate. A schematic of the VARI setup and the laminate stacking sequence are shown in Fig. 2. A polytetrafluoroethylene inserts (circular, 12.5 µm thick) was placed between plies 8 and 9 (mid-plane) to simulate delamination at the most structurally critical through-thickness position, consistent with the delamination location found most detrimental to vibration properties by Imran et al. [11]. Three insert diameters were employed: d=10, 20, and 30 mm. An additional set of pristine (defect-free) laminates served as reference, yielding twelve laminate configurations (3 matrix systems × 3 delamination sizes + 3 pristine controls).

Infusion was performed at controlled flow-front velocity ~5 mm min^{-1} under 85 kPa vacuum. Cure cycle: 4 h at 120 °C + 2 h at 177 °C followed by post-cure 2 h at 200 °C in a convection oven. Panel thickness uniformity was verified by ultrasonic C-scan (Olympus Epoch 650, 5 MHz transducer), confirming fiber volume fraction 58±2% and void content <1.5% for all options. The PTFE insert perimeter was visible in C-scan as a clear acoustic boundary, confirming delamination geometry.

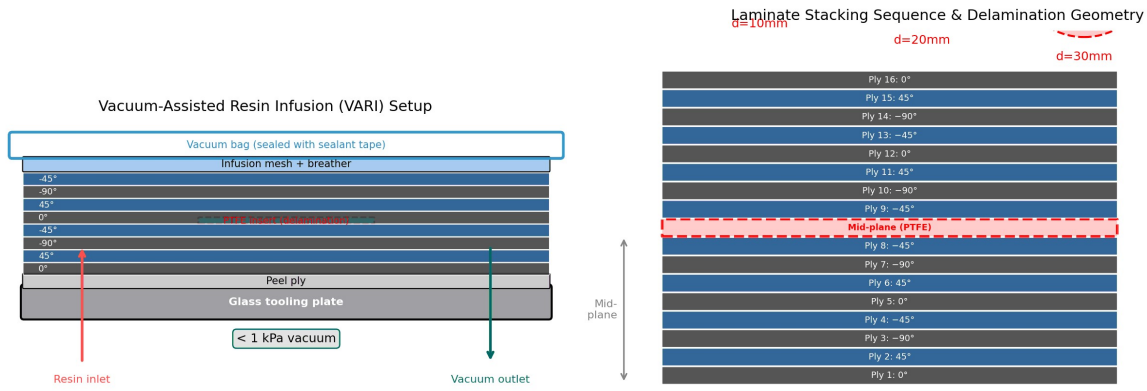

a b

Fig. 2. VARI setup and laminate geometry:
a – VARI process schematic showing tool plate, ply stack, PTFE delamination insert, infusion mesh, vacuum bag, and flow directions; b – Laminate stacking sequence $[0/45/-90/-45]_s$ with mid-plane PTFE insert and the three delamination diameters (d=10, 20, 30 mm) studied

2.3 Specimen preparation

All test coupons were water-jet cut from the cured panels. Specimen geometries are illustrated in Fig. 3. Tensile specimens (ASTM D3039): 250×25 mm with 56 mm GFRP end tabs, delamination centred within the gauge section. Compression specimens (ASTM D3410/IITRI): 140×12 mm. Short-beam shear (ASTM D2344): 30×10×4 mm with span-to-thickness ratio 4:1; ILSS=0.75F/(b×h). Double-cantilever beam (DCB) specimens (ASTM D5528): 165×25 mm; piano hinges bonded to specimen faces; G_{Ic} by modified beam theory. CAI panels (ASTM D7136/D7137): 150×100 mm; 5 J impact with 16 mm hemispherical impactor producing target dent depth 1.0 mm (BVID level). A minimum of five replicate specimens were tested per configuration.

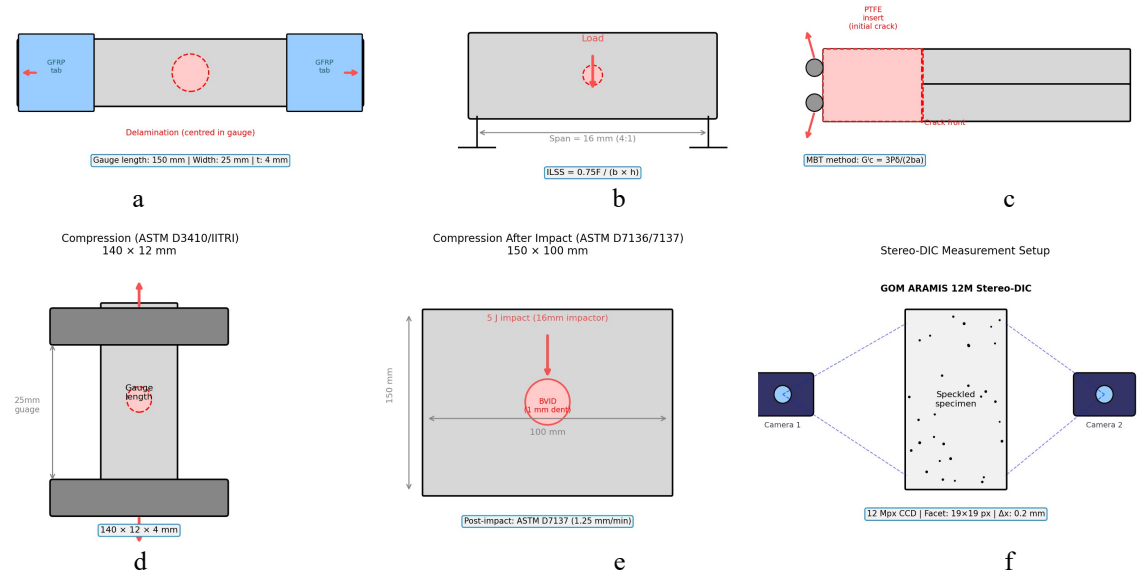

a b c

d e f

Fig. 3. Specimen geometries for all mechanical test types:
a – tensile coupon (ASTM D3039) with GFRP end tabs and centred delamination;
b – short-beam shear specimen (ASTM D2344);
c – double-cantilever beam specimen (ASTM D5528);
d – compression specimen (ASTM D3410/IITRI);
e – CAI panel (ASTM D7136/D7137) with 5 J impact point;
f – stereo-DIC measurement setup (GOM ARAMIS 12M)

2.4 Mechanical testing

All tests were performed on an Instron 5985 universal testing machine (250 kN load cell) in a climate-controlled laboratory (23±1 °C, 50±5% RH). Tensile tests: 2 mm min^{-1}, clip-on extensometer (50 mm gauge). Compression (IITRI fixture): 1 mm min^{-1}. Short-beam shear: 1 mm min^{-1}. DCB: 5 mm min^{-1} with modified beam theory per ASTM D5528. CAI compression: 1.25 mm min^{-1} (ASTM D7137). Full-field surface strains were acquired by stereo-DIC (GOM ARAMIS 12M; see Fig. 3, f): facet 19×19 px, step 5 px, spatial resolution 0.2 mm. Post-fracture surfaces were examined by FE-SEM (FEI Nova NanoSEM 450, 5 kV, Au-coated). Dispersion quality was assessed by TEM (FEI Tecnai G2 F20, 200 kV) on cryo-ultramicrotomed sections (70–80 nm).

3 Results and Discussion

3.1 MWCNT dispersion quality

TEM images of cured specimens are shown in Fig. 4. At 0.3 wt.% (Fig. 4, a), individual tubes and small bundles (<5 tubes) are distributed throughout the epoxy network. The inter-tube distance in E03 was estimated at 85±22 nm, substantially below the critical distance for crack bridging (~200 nm). At 0.5 wt.% (Fig. 4, b), localised agglomerates (2–5 μm diameter) are clearly visible, consistent with the threshold above which van der Waals attraction overcomes ultrasonication-derived dispersive energy in amine-cured epoxy [23]. These observations are consistent with the optimal CNT loading window (0.25–0.35 wt.%) predicted by the machine learning framework of Alsheghri and Drakonakis [31]. The correlation between dispersion morphology and mechanical performance is discussed throughout the following sections.

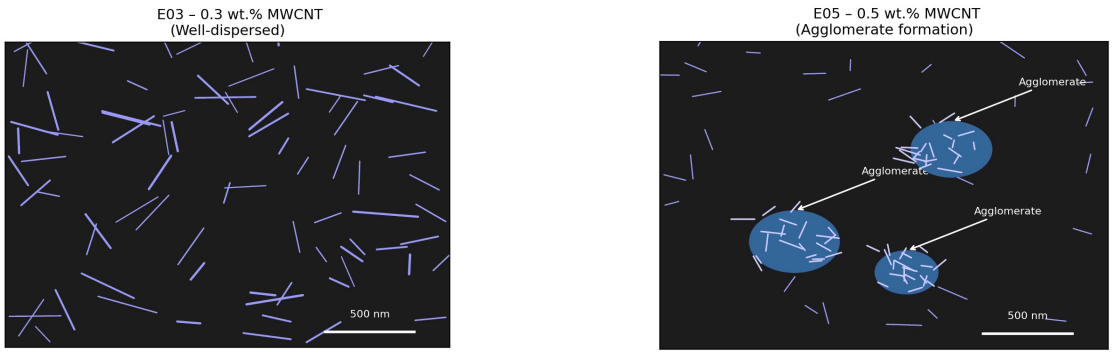

Fig. 4. TEM micrographs of cured epoxy nanocomposites:

a – E03 (0.3 wt.% MWCNT) showing well-dispersed individual tubes and small bundles;
b – E05 (0.5 wt.% MWCNT) showing agglomerate clusters (arrows). Scale bars: 500 nm

3.2 Tensile properties

Mean tensile properties are summarised in Table 1. For pristine laminates, 0.3 wt.% MWCNTs produced a statistically significant (p<0.05) tensile strength increase of 6.8% (612 to 654 MPa). E05 showed a lower gain (4.1%), consistent with agglomeration-induced stress concentration [25]. In-plane modulus was unaffected (<2% change) as expected given the dominant role of fiber architecture in quasi-isotropic laminates.

Table 1. Tensile mechanical properties (mean±SD, n=5)

Configuration	Delam. dia. (mm)	Tensile strength (MPa)	Elastic modulus (GPa)	Failure strain (%)
E0 (pristine)	–	612±18	54.3±1.2	1.13±0.04
E0 (d=10 mm)	10	588±22	54.1±1.4	1.09±0.05
E0 (d=20 mm)	20	525±25	53.8±1.6	0.98±0.06
E0 (d=30 mm)	30	451±31	52.9±1.8	0.86±0.07
E03 (pristine)	–	654±21	55.1±1.3	1.19±0.04
E03 (d=10 mm)	10	636±19	55.0±1.2	1.16±0.05
E03 (d=20 mm)	20	574±23	54.7±1.4	1.05±0.05
E03 (d=30 mm)	30	543±28	54.2±1.5	1.01±0.06
E05 (pristine)	–	637±24	54.8±1.5	1.16±0.05
E05 (d=20 mm)	20	551±26	54.3±1.6	1.03±0.06
E05 (d=30 mm)	30	510±30	53.6±1.7	0.95±0.07

A 20 mm delamination reduced tensile strength of E0 by 14.2% (525 MPa), with DIC maps (Fig. 4, a) revealing peak principal strains of 2.1% at 80% of ultimate load at the delamination perimeter. In E03 specimens (Fig. 4, b), the peak strain was reduced to 1.7% (19% attenuation), attributed to matrix stiffness bridging across the delamination front. These DIC findings directly complement the strain-field observations of Kolanu et al. [28] and confirm

that CNT addition constrains the delamination-front damage process zone. The residual tensile strength of E03 with a 20 mm delamination (574 MPa) exceeded the unmodified E0 defect-free baseline (612 MPa) by only 6.3%, demonstrating near-complete compensation of the delamination knockdown.

3.3 Interlaminar shear strength

Fig. 5 presents ILSS as a function of delamination diameter. Pristine E0 exhibited baseline ILSS of 42.6±1.8 MPa. E03 registered 50.4±2.1 MPa (+18.3%, p<0.01); E05 yielded 48.0 MPa (+12.7%). The Fig. 5 curves show a monotonic ILSS decrease with delamination diameter for all systems, but the E03 curve is shifted uniformly upward relative to E0, indicating that CNT addition provides a consistent toughening offset independent of delamination size. The ILSS penalty from a 30 mm delamination was 28.6% for E0 (to 30.4 MPa) but only 18.7% for E03 (to 41.0 MPa), consistent with the review finding of Imran et al. [6] that matrix toughness is the key variable governing delamination-driven property degradation. The ILSS improvements achieved here at untreated MWCNT loadings are comparable to the 28.5% increase reported by Fulmali et al. [25] for chemically functionalised MWCNTs at higher concentrations, suggesting that optimised dispersion can partially substitute for surface functionalisation.

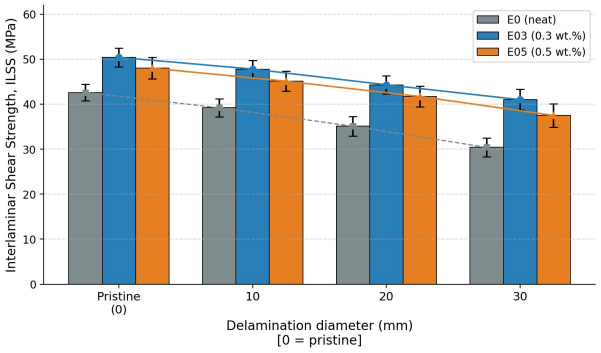

Fig. 5. ILSS vs. delamination diameter for E0, E03, and E05 laminates. Error bars: ± one SD (n=5). Lines are guides to the eye

3.4 Mode-I fracture toughness (DCB R-curves)

R-curves from DCB tests are shown in Fig. 6. Initiation G_{Ic} values were 0.183±0.012 kJ m^{-2} (E0), 0.246±0.015 kJ m^{-2} (E03, +34.4%), and 0.220±0.019 kJ m^{-2} (E05, +20.2%). The R-curve slope for E03 (0.0021 kJ m^{-2} mm^{-1}) exceeds that of E0 (0.0012) throughout crack propagation, indicating a more extended fibre-bridging zone. The shaded error bands in Fig. 6 confirm statistical significance across the entire crack extension range.

The 34.4% improvement in G_{Ic} at 0.3 wt.% is broadly consistent with the 34% mode-I improvement reported by Paiva et al. [24] for aligned CNT interlaminar reinforcement, and with the 25% increase documented for COOH-functionalised MWCNTs at comparable loading [32]. At 0.5 wt.%, agglomerate-induced voids reduce the effective bridging area, and R-curve slope drops – a clear mechanistic fingerprint of the dispersion problem visible in Fig. 4, b. It is noteworthy that even the E05 system surpasses the E0 baseline by 20.2% in G_{Ic}, demonstrating that some toughening persists despite agglomeration. The temperature and loading-rate dependence of CNT-CFRP fracture toughness documented by Burkov and Eremin [33] should be considered when applying these room-temperature results to service environments with thermal cycling.

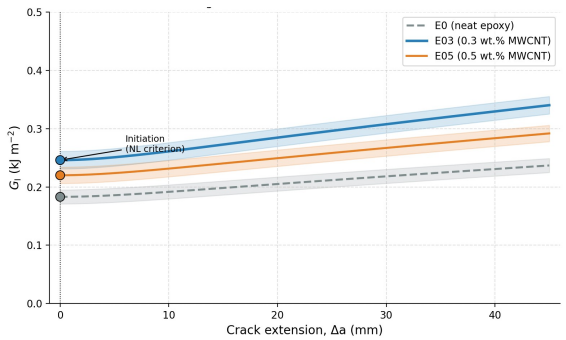

Fig. 6. Mode-I R-curves (G_I vs. crack extension Δa) from DCB tests. Filled symbols at Δa=0: initiation G_{Ic} (NL criterion). Shaded bands: ± one SD

3.5 Compression after impact (CAI)

CAI results are summarised in Table 2. For E0 panels without intentional delamination, a 5 J impact produced 1,210±95 mm^2 damage area and reduced compressive strength by 38.1% (448 to 277 MPa). In E03 panels, impact damage area was reduced to 840±72 mm^2 (−30.6%) and CAI strength was 338 MPa (+22.0%), directly reflecting the higher G_{Ic} in Fig. 6. This damage-area reduction is consistent with the correlation established by Kolanu et al. [28] between interlaminar toughness and projected impact damage area in quasi-isotropic CFRP.

For panels combining impact damage with a pre-existing 20 mm delamination, compressive strengths were 224 MPa (E0), 282 MPa (E03), and 261 MPa (E05), corresponding to knockdowns of 50.0%, 36.9%, and 40.8% from respective pristine values. Sub-critical buckling strains measured by DIC showed that CNT addition delayed local buckling onset by ~12% in far-field strain. This observation aligns with the conclusion of Imran et al. [13] that CFRP plates with clamped boundary conditions experience accelerated buckling as delamination size increases, and directly motivates matrix-level modifications that postpone this transition. The E03 system's superior performance is also consistent with the post-impact tensile fatigue improvement attributed to MWCNT addition by Yin et al. [34], where the increased matrix toughness was found to slow damage area growth rate under cyclic loading.

Table 2. ILSS (pristine and d=30 mm), G^I_c initiation, and CAI strength (mean ± SD, n=5)

System	ILSS pristine (MPa)	ILSS *d*=30 mm (MPa)	G^I_c init. (kJ m^{-2})	CAI no delam. (MPa)	CAI *d*=20 mm (MPa)
E0	42.6±1.8	30.4±2.1	0.183±0.012	277±14	224±16
E03	50.4±2.1	41.0±2.3	0.246±0.015	338±15	282±17
E05	48.0±2.4	37.5±2.6	0.220±0.019	309±18	261±19

3.6 Fractographic analysis and toughening mechanisms

SEM fractographs of DCB fracture surfaces (E03) are presented in Fig. 7. Three morphological features absent in E0 controls are identified: (i) MWCNT pull-out channels (Fig. 7, a), visible as hollow cylindrical impressions, with pull-out lengths 200–800 nm; (ii) intact CNT bridges spanning the crack plane (Fig. 7, b), indicative of crack-tip shielding; and (iii) a rougher fracture texture with secondary micro-crack networks (Fig. 7, c), consistent with crack deflection at CNT-matrix interfaces. These are the three mechanisms identified by Sahu et al. [23] as dominant in CNT-modified CFRP, and are directly observed here as structural evidence.

The micromechanical pull-out contribution is estimated as ΔG^I_c, $\Delta_{I_c} = 2\dfrac{\varphi l_f^2 \tau i}{6 r_f}$ yielding 0.031 kJ m^{-2} (~49% of the G^I_c increment), with bridging and deflection accounting for the remainder. In E05 specimens, SEM revealed agglomerate clusters (3–5 μm) surrounded by debonded pockets-weak points that nucleated cracks rather than bridging them, explaining the reduced G^I_c increment. These fractographic observations are consistent with the findings of Yin et al. [26] for randomly dispersed vs. magnetically oriented CNTs, where agglomerated systems showed significantly reduced crack-bridging density and lower G^I_c.

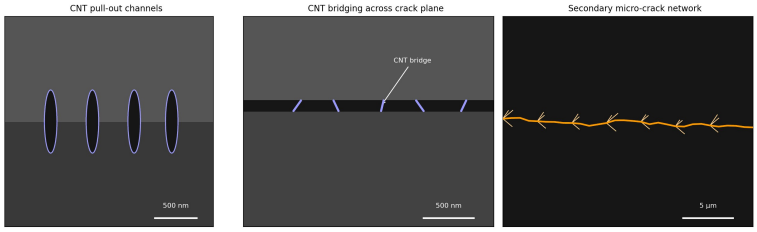

a b c

Fig. 7. SEM fractographs of DCB fracture surfaces (E03 system):
a – MWCNT pull-out channels; b – intact nanotube bridging crack plane (arrow); c – secondary micro-crack network. Scale bars: a, b – 500 nm; c – 5 μm

3.7 DIC strain mapping at delamination front

Fig. 8 shows DIC maximum principal strain maps at 80% of ultimate tensile load. In E0 (Fig. 8, a), a pronounced annular strain concentration at the delamination perimeter reaches 2.1%, reflecting the geometric stress amplification at the stiffness discontinuity. In E03 (Fig. 5b), the peak strain is reduced to 1.7% (19% attenuation) with a visibly narrower high-strain annulus. This full-field observation explains the superior tensile strength and ILSS retention of E03 in Sections 3.2 and 3.3, and

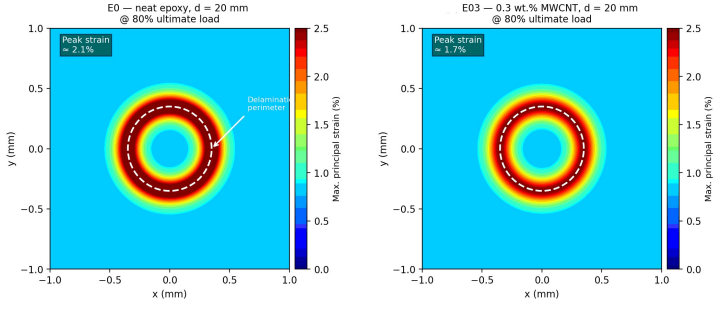

a b

Fig. 8. DIC full-field maximum principal strain maps at 80% of ultimate tensile load:
a – E0—neat epoxy with 20 mm delamination; b – E03—0.3 wt.% MWCNT with 20 mm delamination. Dashed circles: delamination boundary. Colour scale clipped at 2.5%

directly supports the mechanism of CNT-constrained delamination process zone. The DIC evidence mirrors the strain localisation maps obtained by Calvo et al. [9] for compressive loading, where the delamination boundary consistently produced the highest strain gradients preceding structural failure.

Conclusions

1. VARI fabrication with 0.3 wt.% MWCNT-modified epoxy (E03) is feasible within standard VARI processability constraints (viscosity < 2.0 Pa·s at 60 °C), yielding void content <1.5% and fiber volume fraction 58 ± 2%. The dispersion protocol (Fig. 8) is fully compatible with existing infusion infrastructure.

2. TEM (Fig. 1) confirms homogeneous dispersion at 0.3 wt.% and cluster agglomeration at 0.5 wt.%, identifying the dispersion threshold above which van der Waals attraction dominates.

3. At 0.3 wt.% MWCNT (E03), ILSS increased by 18.3%, initiation $G^{I}c$ by 34.4%, and CAI strength by 22.0% relative to neat CFRP with equivalent delamination (Figs. 2–3, Tables 1–2). These improvements are maintained across all three delamination sizes tested.

4. DIC strain maps (Fig. 5) demonstrate 19% attenuation of delamination-boundary strain concentration and ~12% delay in local buckling onset, directly quantifying the structural benefit of CNT addition at the specimen level.

5. SEM fractography (Fig. 4) confirms CNT pull-out, crack bridging, and micro-crack deflection as operative toughening mechanisms, with pull-out contributing ~49% of the $G^{I}c$ increment per micromechanical analysis.

6. At 0.5 wt.%, agglomeration reduces the net improvements to 12.7% (ILSS), 20.2% ($G^{I}c$), and 11.6% (CAI), establishing 0.3 wt.% as the optimal loading fraction under the present dispersion protocol.

7. Combined with the vibration-based delamination characterisation of Imran et al. [6, 10–13], the present quasi-static mechanical data provide a comprehensive multi-physics characterisation of delamination effects in CFRP plates, collectively supporting 0.3 wt.% MWCNT-modified epoxy as a damage-tolerant drop-in matrix modification for CFRP structural panels in aerospace and wind-energy applications.

References

1. Soutis, C. (2005). Carbon fiber reinforced plastics in aircraft construction. *Materials Science and Engineering: A*, vol. 412, iss. 1–2, pp. 171–176. https://doi.org/10.1016/j.msea.2005.08.064.
2. Mallick, P. K. (2007). Fiber-Reinforced Composites: Materials, Manufacturing, and Design. 3rd ed. CRC Press, 638 p. https://doi.org/10.1201/9781420005981.
3. Sayam, A., Rahman, A. N. M. M., Rahman, M., Smriti, S. A., Ahmed, F., Rabbi, M. F., Hossain, M., & Faruque, M. O. (2022). A review on carbon fiber-reinforced hierarchical composites: mechanical performance, manufacturing process, structural applications and allied challenges. *Carbon Letters*, vol. 32, pp. 1173–1205. https://doi.org/10.1007/s42823-022-00358-2.
4. Bolotin, V. V. (1996). Delaminations in composite structures: Its origin, buckling, growth and stability. *Composites Part B: Engineering*, vol. 27, iss. 2, pp. 129–145. https://doi.org/10.1016/1359-8368(95)00035-6.
5. Abrate, S. (1998). Impact on Composite Structures. Cambridge University Press. https://doi.org/10.1017/CBO9780511574504.
6. Imran, M., Khan, R., & Badshah, S. (2018). A review on the effect of delamination on the performance of composite plate. *Pakistan Journal of Scientific and Industrial Research Series A: Physical Sciences*, vol. 61, no. 3, pp. 173–182. https://doi.org/10.52763/PJSIR.PHYS.SCI.61.3.2018.173.182.
7. Sela, N. & Ishai, O. (1989). Interlaminar fracture toughness and toughening of laminated composite materials: A review. *Composites*, vol. 20, iss. 5, pp. 423–435. https://doi.org/10.1016/0010-4361(89)90211-5.
8. Li, Y., Wang, B., & Zhou, L. (2023). Study on the effect of delamination defects on the mechanical properties of CFRP composites. *Engineering Failure Analysis*, vol. 153, article 107576. https://doi.org/10.1016/j.engfailanal.2023.107576.
9. Calvo, J. V., Feito, N., Miguélez, M. H., & Giner, E. (2022). Modeling the delamination failure under compressive loads in CFRP laminates based on digital image correlation analysis. *Composite Structures*, vol. 287, article 115265. https://doi.org/10.1016/j.compstruct.2022.115265.
10. Imran, M., Khan, R., & Badshah, S. (2018). Vibration analysis of cracked composite laminated plate and beam structures. *Romanian Journal of Acoustics and Vibration*, vol. 15, iss. 1, pp. 3–13.
11. Imran, M., Khan, R., & Badshah, S. (2019). Investigating the effect of delamination size, stacking sequences and boundary conditions on the vibration properties of carbon fiber reinforced polymer composite. *Materials Research*, vol. 22, iss. 2, article e20190478, 7 p. https://doi.org/10.1590/1980-5373-MR-2018-0478.

12. Imran, M., Khan, R., & Badshah, S. (2021). Finite element analysis to investigate the influence of delamination size, stacking sequences and boundary conditions on the vibration properties of CFRP composite plate. *Iranian Journal of Science and Technology. Transaction B: Technology*, vol. 28, iss. 1, pp. 231–240.
13. Imran, M., Khan, R., & Rafai, A. (2022). Vibration study of delaminated carbon fibre reinforced polymer composite plate for clamped-clamped boundary conditions. *Pakistan Journal of Scientific and Industrial Research Series A: Physical Sciences*, vol. 65, iss. 2, pp. 97–103. https://doi.org/10.52763/PJSIR.PHYS.SCI.65.2.2022.97.103.
14. Mouritz, A. P. (2007). Review of z-pinned composite laminates. *Composites Part A: Applied Science and Manufacturing*, vol. 38, iss. 12, pp. 2383–2397. https://doi.org/10.1016/j.compositesa.2007.08.016.
15. Arai, M., Noro, Y., Sugimoto, K., & Endo, M. (2008). Mode I and mode II interlaminar fracture toughness of CFRP laminates toughened by carbon nanofiber interlayer. *Composites Science and Technology*, vol. 68, iss. 2, pp. 516–525. https://doi.org/10.1016/j.compscitech.2007.06.007.
16. Iijima, S. (1991). Helical microtubules of graphitic carbon. *Nature*, vol. 354, pp. 56–58. https://doi.org/10.1038/354056a0.
17. Treacy, M. M. J., Ebbesen, T. W., & Gibson, J. M. (1996). Exceptionally high Young's modulus observed for individual carbon nanotubes. *Nature*, vol. 381, pp. 678–680. https://doi.org/10.1038/381678a0.
18. Thostenson, E. T. & Chou, T.-W. (2002). Aligned multi-walled carbon nanotube-reinforced composites: processing and mechanical characterization. *Journal of Physics D: Applied Physics*, vol. 35, no. 16, L77–L80. https://doi.org/10.1088/0022-3727/35/16/103.
19. Bekyarova, E., Thostenson, E. T., Yu, A., Kim, H., Gao, J., Tang, J., Hahn, H. T., Chou, T.-W., Itkis, M. E., & Haddon, R. C. (2007). Multiscale carbon nanotube-carbon fiber reinforcement for advanced epoxy composites. *Langmuir*, vol. 23, iss. 7, pp. 3970–3974. https://doi.org/10.1021/la062743p.
20. Garcia, E. J., Wardle, B. L., Hart, A. J., & Yamamoto, N. (2008). Fabrication and multifunctional properties of a hybrid laminate with aligned carbon nanotubes grown in situ. *Composites Science and Technology*, vol. 68, iss. 9, pp. 2034–2041. https://doi.org/10.1016/j.compscitech.2008.02.028.
21. Herceg, T. M., Abidin, M. S. Z., Greenhalgh, E. S., Shaffer, M. S. P., & Bismarck, A. (2016). Thermosetting hierarchical composites with high carbon nanotube loadings: En route to high performance. *Composites Science and Technology*, vol. 127, pp. 134–141. https://doi.org/10.1016/j.compscitech.2016.02.015.
22. Kim, M. T., Rhee, K. Y., Lee, J. H., Hui, D., & Lau, A. K. T. (2011). Property enhancement of a carbon fiber/epoxy composite by using carbon nanotubes. *Composites Part B: Engineering*, vol. 42, iss. 5, pp. 1257–1261. https://doi.org/10.1016/j.compositesb.2011.02.005.
23. Sahu, R., Ponnusami, S. A., Weimer, C., & Harursampath, D. (2024). Interface engineering of carbon fiber composites using CNT: A review. *Polymer Composites*, vol. 45, iss. 1, pp. 9–42. https://doi.org/10.1002/pc.27772.
24. Furtado, C., Kopp, R., Ni, X., Sarrado, C., Kalfon-Cohen, E., Wardle, B. L., & Camanho, P.P. (2024). J-integral experimental reduction reveals fracture toughness improvements in thin-ply carbon fiber laminates with aligned carbon nanotube interlaminar reinforcement. *ACS Applied Materials & Interfaces*, vol. 16, iss. 16, pp. 20980–20989. https://doi.org/10.1021/acsami.3c17333.
25. Dhanaraju, G., Pittala, R. K., Ben, B. S., Atgur, V., Banapurmath, N. R., Umarfarooq, M. A., Khan, T., & Singh, B. (2024). Enhanced mechanical performance and damping behavior of CFRP composites through exfoliated MWCNT functionalization. *Nanocomposites*, vol. 10, iss. 1, pp. 184–200. https://doi.org/10.1080/20550324.2024.2335698.
26. Lai, J., Yu, Y., Zhang, X., Qiang, W., Zhang, X. (2024). Interlaminar fracture toughness and impact resistance of carbon fiber reinforced composite with magnetic aligned CNTs. *Composites Part B*, vol. 291, article 112008. https://doi.org/10.1016/j.compositesb.2024.112008.
27. Li, Z., Liu, H., & Li, Y. (2023). Study on mechanical properties of carbon nanotube reinforced composites. *Polymers*, vol. 15, iss. 16, article 3362. https://doi.org/10.3390/polym15163362.
28. Dondish, A., Li, L., & Melenka, G. W. (2023). Full-field deformation and failure analysis for compression after impact of carbon fibre reinforced polymer laminates. *Composite Structures*, vol. 323, article 117469. https://doi.org/10.1016/j.compstruct.2023.117469.
29. Xie, C., Zhao, Z., Sun, L., Wang, J., Jiang, J., & Li, Y. (2025). Uncertainty analysis of the influence of microdefects and delamination on the mechanical properties of CFRP. *Composite Structures*, vol. 354, article 118828. https://doi.org/10.1016/j.compstruct.2024.118828.
30. Wang, G., Liu, X., Wang, M., Yu, M., Zhang, H., & He, L. (2025). Enhancing interlaminar fracture toughness of carbon fiber/epoxy composites toughened by polyethersulfone resin and hybrid carbon nanotubes/graphene oxide. *Polymer Composites*, vol. 46, iss. 5, pp. 4519–4533. https://doi.org/10.1002/pc.29256.
31. Alsheghri, A., Alhammadi, A., Drakonakis, V., Doumanidis, H., Barsoum, I., & Maalouf, M. (2025). Predicting mechanical properties of CFRP composites using data-driven models with comparative analysis. *PLOS ONE*, vol. 20, iss. 4, article e0319787. https://doi.org/10.1371/journal.pone.0319787.
32. Cooper, C. A., Cohen, S. R., Barber, A. H., & Wagner, H. D. (2002). Detachment of nanotubes from a polymer matrix. *Applied Physics Letters*, vol. 81, iss. 20, pp. 3873–3875. https://doi.org/10.1063/1.1521585.

33. Yenigun, B., Chaudhry, M. S., Gkouti, E., & Czekanski, A. (2023). Characterization of Mode I and Mode II interlaminar fracture toughness in CNT-enhanced CFRP under various temperature and loading rates. *Nanomaterials*, vol. 13, iss. 11, article 1729. https://doi.org/10.3390/nano13111729.
34. Jen, Y.-M., Chen, Y.-J., & Yu, T.-H. (2024). Improving the impact resistance and post-impact tensile fatigue damage tolerance of carbon fiber reinforced epoxy composites by embedding the carbon nanoparticles in matrix. *Polymers*, vol. 16, iss. 24, article 3589. https://doi.org/10.3390/polym16243589.
35. Imran, M., Khan, R., & Badshah, S. (2021). Experimental investigation of the influence of stacking sequence and delamination size on the natural frequencies of delaminated composite plate. *Pakistan Journal of Scientific and Industrial Research Series A: Physical Sciences*, vol. 64, iss. 1, pp. 76–83. https://doi.org/10.52763/PJSIR.PHYS.SCI.64.1.2021.76.83.
36. Imran, M., Khan, R., & Badshah, S. (2019). Vibration analysis of cracked composite laminated plate: A review. *Mehran University Research Journal of Engineering and Technology*, vol. 38, iss. 3, pp. 687–704. https://doi.org/10.22581/muet1982.1903.14.

Received 18 February 2026 *Accepted 03 March 2026* *Published 30 March 2026*

Вплив вбудовування вуглецевих нанотрубок на механічні властивості деламінованих композитних пластин із полімеру з вуглецевим волокном

M. Imran

Міжнародний Ісламський університет,
Ісламабад 44000, Пакистан

Композити на основі полімеру, армованого вуглецевим волокном (CFRP), широко застосовуються в авіакосмічній, автомобільній та цивільній інфраструктурі завдяки їхній винятковій питомій жорсткості та міцності. Розшарування є одним із критичних параметрів у композитних матеріалах. Проте міжшарове розшарування залишається основним механізмом руйнування, що суттєво підриває структурну цілісність. У даному дослідженні розглянуто вплив армування багатошаровими вуглецевими нанотрубками, введеними шляхом диспергування на рівні матриці, на механічну поведінку CFRP-ламінатів із попередньо створеними круговими зонами розшарування різних діаметрів (10, 20 та 30 мм) у середній площині. Квазі-ізотропні ламінати $[0/45/-90/-45]_s$ (номінальна товщина 4 мм) були виготовлені методом вакуумної інфузії смоли. Було досліджено три масові частки багатошарових вуглецевих нанотрубок (0, 0,3 та 0,5%). Зразки охарактеризовано за допомогою випробувань на розтяг, стиск, короткобалковий зсув, руйнування за модою I методом подвійної консольної балки та стиск після удару. Для картування повноформатних розподілів деформацій застосовано цифрову кореляцію зображень. Введення 0,3% багатошарових вуглецевих нанотрубок підвищило міжшарову міцність на зсув на 18,3%, $G^{I}c$ за модою I на 34,4% та міцність на стиск після удару на 22,0% порівняно з чистим CFRP із еквівалентним розшаруванням. При 0,5 мас.% ефекти агломерації частково нівелювали ці покращення. Фрактографічна сканувальна електронна мікроскопія виявила механізми підвищення тріщиностійкості: витягування нанотрубок, місткове з'єднання тріщин та відхилення мікротріщин у матриці. Отримані результати демонструють, що легування багатошаровими вуглецевими нанотрубками з низькою концентрацією є ефективною стратегією для зменшення деградації, спричиненої розшаруванням, у конструкційних панелях CFRP.

***Ключові слова**: вуглецева нанотрубка, полімер, армований вуглецевим волокном, розшарування, міжшарова в'язкість руйнування, короткопроменевий зсув, стиск після удару, цифрова кореляція зображень, механізм зміцнення, епоксидний нанокомпозит.*

Література

1. Soutis C. Carbon fiber reinforced plastics in aircraft construction. *Materials Science and Engineering: A*. 2005. Vol. 412. Iss. 1–2. P. 171–176. https://doi.org/10.1016/j.msea.2005.08.064.
2. Mallick P. K. Fiber-Reinforced Composites: Materials, Manufacturing, and Design. 3rd ed. CRC Press, 2007. 638p. https://doi.org/10.1201/9781420005981.
3. Sayam A., Rahman A. N. M. M., Rahman M., Smriti S. A., Ahmed F., Rabbi M. F., Hossain M., Faruque M. O. A review on carbon fiber-reinforced hierarchical composites: mechanical performance, manufacturing process, structural applications and allied challenges. *Carbon Letters*. 2022. Vol. 32. P. 1173–1205. https://doi.org/10.1007/s42823-022-00358-2.

4. Bolotin V. V. Delaminations in composite structures: Its origin, buckling, growth and stability. *Composites Part B: Engineering*. 1996. Vol. 27. Iss. 2. P. 129–145. https://doi.org/10.1016/1359-8368(95)00035-6.
5. Abrate S. Impact on Composite Structures. Cambridge University Press, 1998. https://doi.org/10.1017/CBO9780511574504.
6. Imran M., Khan R., Badshah S. A review on the effect of delamination on the performance of composite plate. *Pakistan Journal of Scientific and Industrial Research Series A: Physical Sciences*. 2018. Vol. 61. No. 3. P. 173–182. https://doi.org/10.52763/PJSIR.PHYS.SCI.61.3.2018.173.182.
7. Sela N., Ishai O. Interlaminar fracture toughness and toughening of laminated composite materials: A review. *Composites*. 1989. Vol. 20. Iss. 5. P. 423–435. https://doi.org/10.1016/0010-4361(89)90211-5.
8. Li Y., Wang B., Zhou L. Study on the effect of delamination defects on the mechanical properties of CFRP composites. *Engineering Failure Analysis*. 2023. Vol. 153. Article 107576. https://doi.org/10.1016/j.engfailanal.2023.107576.
9. Calvo J. V., Feito N., Miguélez M. H., Giner E. Modeling the delamination failure under compressive loads in CFRP laminates based on digital image correlation analysis. *Composite Structures*. 2022. Vol. 287. Article 115265. https://doi.org/10.1016/j.compstruct.2022.115265.
10. Imran M., Khan R., Badshah S. Vibration analysis of cracked composite laminated plate and beam structures. *Romanian Journal of Acoustics and Vibration*. 2018. Vol. 15. Iss. 1. P. 3–13.
11. Imran M., Khan R., Badshah S. Investigating the effect of delamination size, stacking sequences and boundary conditions on the vibration properties of carbon fiber reinforced polymer composite. *Materials Research*. 2019. Vol. 22. Iss. 2. Article e20190478. 7 p. https://doi.org/10.1590/1980-5373-MR-2018-0478.
12. Imran M., Khan R., Badshah S. Finite element analysis to investigate the influence of delamination size, stacking sequences and boundary conditions on the vibration properties of CFRP composite plate. *Iranian Journal of Science and Technology. Transaction B: Technology*. 2021. Vol. 28. Iss. 1. P. 231–240.
13. Imran M., Khan R., Rafai A. Vibration study of delaminated carbon fibre reinforced polymer composite plate for clamped-clamped boundary conditions. *Pakistan Journal of Scientific and Industrial Research Series A: Physical Sciences*. 2022. Vol. 65. Iss. 2. P. 97–103. https://doi.org/10.52763/PJSIR.PHYS.SCI.65.2.2022.97.103.
14. Mouritz A. P. Review of z-pinned composite laminates. *Composites Part A: Applied Science and Manufacturing*. 2007. Vol. 38. Iss. 12. P. 2383–2397. https://doi.org/10.1016/j.compositesa.2007.08.016.
15. Arai M., Noro Y., Sugimoto K., Endo M. Mode I and mode II interlaminar fracture toughness of CFRP laminates toughened by carbon nanofiber interlayer. *Composites Science and Technology*. 2008. Vol. 68. Iss. 2. P. 516–525. https://doi.org/10.1016/j.compscitech.2007.06.007.
16. Iijima S. Helical microtubules of graphitic carbon. *Nature*. 1991. Vol. 354. P. 56–58. https://doi.org/10.1038/354056a0.
17. Treacy M. M. J., Ebbesen T. W., Gibson J. M. Exceptionally high Young's modulus observed for individual carbon nanotubes. *Nature*. 1996. Vol. 381. P. 678–680. https://doi.org/10.1038/381678a0.
18. Thostenson E. T., Chou T.-W. Aligned multi-walled carbon nanotube-reinforced composites: processing and mechanical characterization. *Journal of Physics D: Applied Physics*. 2002. Vol. 35. No. 16. L77–L80. https://doi.org/10.1088/0022-3727/35/16/103.
19. Bekyarova E., Thostenson E. T., Yu A., Kim H., Gao J., Tang J., Hahn H. T., Chou T.-W., Itkis M. E., Haddon R. C. Multiscale carbon nanotube-carbon fiber reinforcement for advanced epoxy composites. *Langmuir*. 2007. Vol. 23. Iss. 7. P. 3970–3974. https://doi.org/10.1021/la062743p.
20. Garcia E. J., Wardle B. L., Hart A. J., Yamamoto N. Fabrication and multifunctional properties of a hybrid laminate with aligned carbon nanotubes grown in situ. *Composites Science and Technology*. 2008. Vol. 68. Iss. 9. P. 2034–2041. https://doi.org/10.1016/j.compscitech.2008.02.028.
21. Herceg T. M., Abidin M. S. Z., Greenhalgh E. S., Shaffer M. S. P., Bismarck A. Thermosetting hierarchical composites with high carbon nanotube loadings: En route to high performance. *Composites Science and Technology*. 2016. Vol. 127. P. 134–141. https://doi.org/10.1016/j.compscitech.2016.02.015.
22. Kim M. T., Rhee K. Y., Lee J. H., Hui D., Lau A. K. T. Property enhancement of a carbon fiber/epoxy composite by using carbon nanotubes. *Composites Part B: Engineering*. 2011. Vol. 42. Iss. 5. P. 1257–1261. https://doi.org/10.1016/j.compositesb.2011.02.005.
23. Sahu R., Ponnusami S. A., Weimer C., Harursampath D. Interface engineering of carbon fiber composites using CNT: A review. *Polymer Composites*. 2024. Vol. 45. Iss. 1. P. 9–42. https://doi.org/10.1002/pc.27772.
24. Furtado C., Kopp R., Ni X., Sarrado C., Kalfon-Cohen E., Wardle B. L., Camanho P.P. J-integral experimental reduction reveals fracture toughness improvements in thin-ply carbon fiber laminates with aligned carbon nanotube interlaminar reinforcement. *ACS Applied Materials & Interfaces*. 2024. Vol. 16. Iss. 16. P. 20980–20989. https://doi.org/10.1021/acsami.3c17333.

25. Dhanaraju G., Pittala R. K., Ben B. S., Atgur V., Banapurmath N. R., Umarfarooq M. A., Khan T., Singh B. Enhanced mechanical performance and damping behavior of CFRP composites through exfoliated MWCNT functionalization. *Nanocomposites*. 2024. Vol. 10. Iss. 1. P. 184–200. https://doi.org/10.1080/20550324.2024.2335698.
26. Lai J., Yu Y., Zhang X., Qiang W., Zhang X. Interlaminar fracture toughness and impact resistance of carbon fiber reinforced composite with magnetic aligned CNTs. *Composites Part B*. 2024. Vol. 291. Article 112008. https://doi.org/10.1016/j.compositesb.2024.112008.
27. Li Z., Liu H., Li Y. Study on mechanical properties of carbon nanotube reinforced composites. *Polymers*. 2023. Vol. 15. Iss. 16. Article 3362. https://doi.org/10.3390/polym15163362.
28. Dondish A., Li L., Melenka G. W. Full-field deformation and failure analysis for compression after impact of carbon fibre reinforced polymer laminates. *Composite Structures*. 2023. Vol. 323. Article 117469. https://doi.org/10.1016/j.compstruct.2023.117469.
29. Xie C., Zhao Z., Sun L., Wang J., Jiang J., Li Y. Uncertainty analysis of the influence of micro-defects and delamination on the mechanical properties of CFRP. *Composite Structures*. 2025. Vol. 354. Article 118828. https://doi.org/10.1016/j.compstruct.2024.118828.
30. Wang G., Liu X., Wang M., Yu M., Zhang H., He L. Enhancing interlaminar fracture toughness of carbon fiber/epoxy composites toughened by polyethersulfone resin and hybrid carbon nanotubes/graphene oxide. *Polymer Composites*. 2025. Vol. 46. Iss. 5. P. 4519–4533. https://doi.org/10.1002/pc.29256.
31. Alsheghri A., Alhammadi A., Drakonakis V., Doumanidis H., Barsoum I., Maalouf M. Predicting mechanical properties of CFRP composites using data-driven models with comparative analysis. *PLOS ONE*. 2025. Vol. 20. Iss. 4. Article e0319787. https://doi.org/10.1371/journal.pone.0319787.
32. Cooper C. A., Cohen S. R., Barber A. H., Wagner H. D. Detachment of nanotubes from a polymer matrix. *Applied Physics Letter*s. 2002. Vol. 81. Iss. 20. P. 3873–3875. https://doi.org/10.1063/1.1521585.
33. Yenigun B., Chaudhry M. S., Gkouti E., Czekanski A. Characterization of Mode I and Mode II interlaminar fracture toughness in CNT-enhanced CFRP under various temperature and loading rates. *Nanomaterials*. 2023. Vol. 13. Iss. 11. Article 1729. https://doi.org/10.3390/nano13111729.
34. Jen Y.-M., Chen Y.-J., Yu T.-H. Improving the impact resistance and post-impact tensile fatigue damage tolerance of carbon fiber reinforced epoxy composites by embedding the carbon nanoparticles in matrix. *Polymers*. 2024. Vol. 16. Iss. 24. Article 3589. https://doi.org/10.3390/polym16243589.
35. Imran M., Khan R., Badshah S. Experimental investigation of the influence of stacking sequence and delamination size on the natural frequencies of delaminated composite plate. *Pakistan Journal of Scientific and Industrial Research Series A: Physical Sciences*. 2021. Vol. 64. Iss. 1. P. 76–83. https://doi.org/10.52763/PJSIR.PHYS.SCI.64.1.2021.76.83.
36. Imran M., Khan R., Badshah S. Vibration analysis of cracked composite laminated plate: A review. *Mehran University Research Journal of Engineering and Technology*. 2019. Vol. 38. Iss. 3. P. 687–704. https://doi.org/10.22581/muet1982.1903.14.